A Model to Monitor Cracked Reinforced Concrete Structures Using Coda Waves

FELIX CLAUß, MARK ALEXANDER AHRENS
and PETER MARK

ABSTRACT

Monitoring of reinforced concrete structures is of paramount importance in ensuring structural health and reliability. To this end, this paper formulates a novel model for evaluating cracked reinforced concrete structures using ultrasonic coda waves. The proposed ε_{sm}-dv/v model combines the well-established σ_s-ε_{sm} relationship with the highly sensitive ultrasonic coda waves, allowing the prediction of strains in the reinforcement independent of geometry, material, and reinforcement ratio. After derivation, the proposed model is validated by experiments on reinforced concrete beams with different dimensions and concrete properties. The results show that the model accurately predicts strains in the reinforcement and thus offers great potential for practical applications in monitoring of reinforced concrete structures.

INTRODUCTION

Reinforced concrete (RC) is the world's most widely used building material. Its health is largely determined by the width of cracks in the concrete, which depends on the strain of the reinforcement. Monitoring this reinforcement strain is, therefore, the most efficient way to detect deficient zones in structures and quantify the extent of potential damage. Damage detected at an early stage can then be repaired easily and quickly, thus maintaining the structure in the long term. A broad range of methods are suitable for monitoring. These include classic methods such as strain gauges or displacement transducers and newer ones such as fiber optic sensors (FOS) and ultrasound. Ultrasonic (US) methods include those based on coda waves [1]. The coda is the late part of a US signal sent from a transmitter to one or more receivers. Its waves are scattered many times in the material, travel through large volumes, and pick up information about strains [2–4], cracks [5–7], temperatures [8], and moisture [9]. Changes in these influences contained in the signal are revealed by coda wave interferometry (CWI) [10].

The paper utilizes a resultant quantity of CWI: the relative velocity change dv/v. In [11], it was recognized that this is proportional to the average strain in the flexural

Felix Clauß, Mark Alexander Ahrens, Peter Mark; Institute of Concrete Structures, Faculty of Civil and Environmental Engineering, Ruhr University Bochum, Universitatsstraße 150, 44801 Bochum, Germany

reinforcement. This is exploited in a model for monitoring RC structures. The average strain is mathematically transformed via well-established methods into the strain of the flexural reinforcement in the crack, which is decisive for assessing the health of RC structures. The theoretical model is validated by lab experiments and evaluated with respect to its accuracy.

MODEL BASICS AND DERIVATION

Coda Wave Interferometry

In heterogeneous media such as concrete, US waves scatter depending on the wave properties as well as those of the inhomogeneities. Due to the scattering, a part of the waves is deflected from the direct path between transmitter and receiver, passes through larger volumes, and reaches the receiver with a delay. The late part of the US signal is called the coda (cf. figure 1). Changes in the material due to mechanical strain, temperature, humidity, or cracks directly alter the recorded signal.

CWI compares sequential US measurements in the time interval $[t_1, t_2]$. For this purpose, the stretching technique of CWI (equation 1) is applied here. This method successively stretches the reference signal by factors ε. The stretching factor that maximizes the cross-correlation coefficient CC is the negative relative velocity change dv/v. The cross-correlation coefficient determines the similarity of the reference $u_1(t)$ to a modified signal $u_2(t)$. The reference measurement may be fixed for an experiment or changed as it proceeds. If large changes are expected as due to cracks in the concrete, the changing reference [12] is recommended.

$$-\frac{dv}{v} = \underset{\varepsilon\in\mathbb{R}}{\arg\max}\, CC(t,\varepsilon) = \underset{\varepsilon\in\mathbb{R}}{\arg\max}\, \frac{\int_{t_1}^{t_2} u_1(t(1-\varepsilon))\, u_2(t)\ \mathrm{d}t}{\sqrt{\int_{t_1}^{t_2} u_1^2(t(1-\varepsilon))\ \mathrm{d}t \int_{t_1}^{t_2} u_2^2(t)\ \mathrm{d}t}} \tag{1}$$

Tension Stiffening

In principle, the load-bearing behavior of RC can be characterized by the state of the concrete (I: non-cracked or II: cracked, cf. indices in equations 2 to 4). In the non-

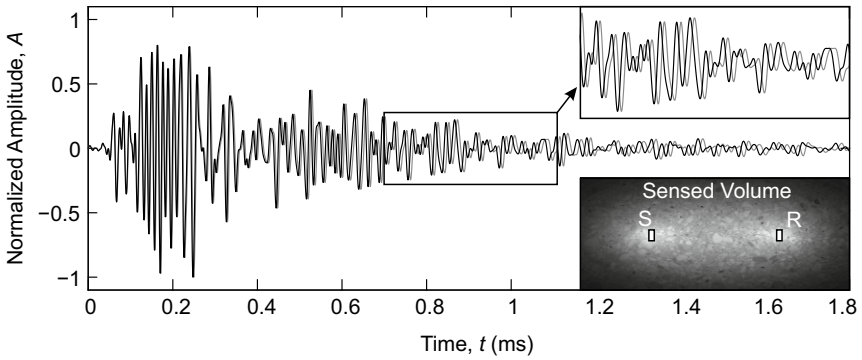

Figure 1. Two US signals (before and after an event) with zoom on coda part.

cracked, linear-elastic state, the concrete carries both compressive and tensile stresses. When the tensile strength of the concrete is exceeded, the first cracks appear, and the concrete henceforth bears only the compressive stresses. The tensile stresses released with cracking are introduced into the reinforcement via bond. A stress peak occurs in the reinforcement in the crack. As the distance from the crack increases, the stress is transferred back into the concrete again via bond. This results in the well-known variable stress curve in the reinforcement with peaks at the positions of cracks in the concrete.

An established approach that captures the load-bearing behavior of RC is the steel stress–average strain relationship (σ_s-ε_{sm}) of the reinforcement [13, 14]. In general, this relationship idealizes four ranges across the stress in the reinforcement σ_s. The starting point is the linear-elastic range 1. The stress in the reinforcement is less than the stress required to produce the first crack in the concrete σ_{sr}^{I}. Without cracks, the average steel strain is the local steel ε_s.

Range 1: $0 \leq \sigma_s \leq \sigma_{sr}^{I}$:

$$\varepsilon_{sm} = \varepsilon_s \tag{2}$$

If the tensile strength of the concrete is exceeded, the concrete cracks. Due to the then lower moment of inertia of the cross-section, the stress in the reinforcement increases suddenly to σ_{sr}^{II}. The strain in the reinforcement also increases in the vicinity of the crack ($\Delta\varepsilon_{sr}$). Mathematically, this region is modeled by interpolating the average strains of ranges 1 and 3. The factor β_t captures the bond quality of the reinforcement. The corresponding terms in equation 3–5 account for tension stiffening.

Range 2: $\sigma_{sr}^{II} < \sigma_s \leq 1.3\,\sigma_{sr}^{II}$:

$$\varepsilon_{sm} = \varepsilon_s - \frac{\beta_t(\sigma_s - \sigma_{sr}^{II}) + (1.3\,\sigma_{sr}^{II} - \sigma_s)}{0.3\,\sigma_{sr}^{II}}\Delta\varepsilon_{sr} \tag{3}$$

In the third range, crack formation is completed. All possible cracks have formed. When the load further increases, just the force in the reinforcement is increased via the bond. As a result, the reinforcement is stretched, and the cracks become wider. This range ends with the yielding of the reinforcement f_y. Then, approx. 90% of the maximum load-bearing capacity is reached.

Range 3: $1.3\,\sigma_{sr}^{II} < \sigma_s \leq f_y$:

$$\varepsilon_{sm} = \varepsilon_s - \beta_t\,\Delta\varepsilon_{sr} \tag{4}$$

In range 4, the strain of the steel is so large that the reinforcement yields. The relation σ_s-ε_{sm} is characterized by the hardening of the reinforcement steel. Thereby, δ_d accounts for the ductility of the reinforcement. The range ends with the failure of the reinforcement at f_t.

Range 4: $f_y < \sigma_s \leq f_t$

$$\varepsilon_{sm} = \varepsilon_{sy} - \beta_t\,\Delta\varepsilon_{sr} + \delta_d\left(1 - \frac{\sigma_{sr}^{II}}{f_y}\right)(\varepsilon_s - \varepsilon_{sy}) \tag{5}$$

Model Proposal: ε_s-dv/v Model

The derivation of the proposed model here is based on the proportionality of the average steel strain and the relative velocity change of coda waves in RC structures already recognized in [11]:

$$\varepsilon_{sm} \propto dv/v \tag{6}$$

This proportionality connects quantities of coda waves (especially the relative velocity change) with the actual strain state in RC members. For this purpose, the proportionality constant c is first introduced. However, in contrast to [11], it is interpreted here as a superordinate constant that is independent of geometry, concrete, or reinforcement ratio. By transforming equations 2 and 6, equation 7 follows for the linear-elastic range. Similarly, the limits of the σ_s-ε_{sm} relation have to be reformulated. They result from division by c.

Range 1: $0 \leq dv/v \leq \varepsilon_{sr}^{I}/c$

$$\varepsilon_s = c \cdot dv/v \tag{7}$$

In general, β_t takes into account not only the type (short- or long-term) but also the level of stress [13, 14]. Here, $\beta_t = 1.0$ is set. This greatly simplifies the model, but the actual strain ε_s is only slightly overestimated. Thus, the calculation of ε_s is always on the safe side. By this idealization, the equations 3 and 4 become identical. Inserting the proportionality relation yields a continuous formulation in which the upper limit is defined by the average yield strength of the reinforcing steel ε_{sym}:

Range 2: $\varepsilon_{sr}^{I}/c \leq dv/v \leq \varepsilon_{sym}/c = (\varepsilon_{sy} - \Delta\varepsilon_{sr})/c$

$$\varepsilon_s = c \cdot dv/v + \Delta\varepsilon_{sr} \tag{8}$$

With the yielding of the reinforcement, approx. 90% of the load-bearing capacity is reached. Since no constant load plateau can be kept in tests when the reinforcement yields (cf. figure 3), the model can unfortunately not be validated beyond the third range. So, its range of application ends here.

Universal Calibration

EXPERIMENTS

To calibrate and validate the proposed model, two tests were performed on large-sized RC beams (specimens 1 and 2) subjected to four-point bending (see figure 2). Both have rectangular cross-sections with different dimensions (width w, depth d, span l, spacing of loads l_F), reinforcement amounts (flexural A_{s1} and constructive A_{s2}, associated effective covers d_1 / d_2, stirrups a_{sw}). They are listed besides the material parameters (Young's modulus of concrete E_{cm}, compressive strength of concrete cubes $f_{cm,cube}$, concrete tensile strength f_{ctm}, Young's modulus of reinforcement E_{sm}, yield strength of reinforcement f_{ym}, tensile strength of reinforcement f_{tm}) in tables I and II. All material parameters were determined from accompanying tests as the mean of three individual samples.

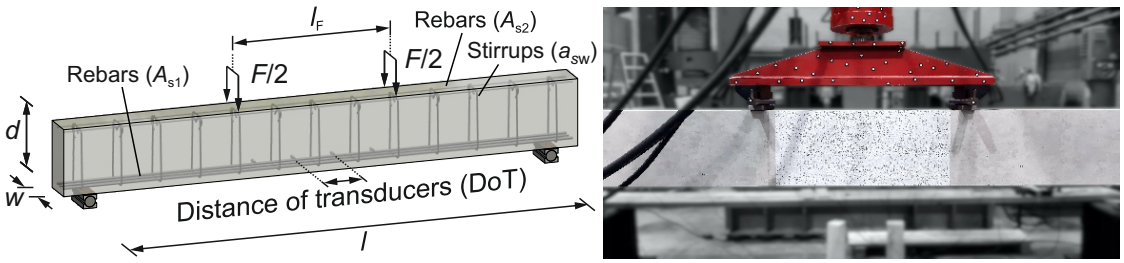

Figure 2. Left: Drawing of the test specimens with dimensions, Right: Photo of test specimen 2 just before the test.

TABLE I. DIMENSIONS OF TEST SPECIMENS

	w (m)	d (m)	l (m)	A_{s1} (cm^2)	d_1 (m)	A_{s2} (cm^2)	d_2 (m)	a_{sw} (cm^2/m)	DoT (m)	#T (-)	l_F (m)
1	0.15	0.4	2.0	4.02	0.038	1.0	0.034	7.85	0.2	5	0.66
2	0.25	0.5	3.5	9.42	0.044	1.0	0.038	7.54	0.3	4	1.20

In the central region of constant bending below the loads, strains were measured with FOS and US transducers. Number (#T) and spacing (DoT) of embedded US transducers (Acoustic Control Systems Ltd., type SO807) are given in table I. They consist of a piezoceramic cylinder and have a central frequency of about 60 kHz.

In general, FOS can accurately record strain and temperature changes at sub-millimeter increments. Prior to this study, the FOS were characterized in detail in [15–17] with respect to their use, application, accuracy, and strain and temperature coupling. A polyimide-coated FOS was bonded to the flexural reinforcement using Polytec PT AC 2411 two-component adhesive. Thus, the FOS continuously record the longitudinal strain of the reinforcement of the entire test specimen.

Figure 2 shows the load-controlled tests. The load was increased step-wise (see figure 3). On each level, it was kept constant for a short time in order to perform the US measurements. Both test specimens were loaded up to the calculated yielding of the reinforcement (specimen 1: 160 kN and specimen 2: 300 kN). Temperature and humidity were kept constant throughout.

CALIBRATION

From the measured data, the constant c can be derived universally. For this purpose, figure 3 compares the relative velocity change (experimental) with the corresponding average strain (analytical from σ_s-ε_{sm} relation). As noted in [11], the data appear linearly correlated. Linear regression yields $c = 205$ µstrain/%. With a coefficient of determination of $R^2 = 0.97$ and an RMSE $= 102$ µstrain (root mean squared error), the average strain is quite accurately captured by the relative velocity change.

TABLE II. MATERIAL PARAMETERS OF TEST SPECIMENS (MPA)

	E_{cm}	$f_{cm,cube}$	f_{ctm}	E_{sm}	f_{ym}	f_{tm}
1	28,600	35.0	2.5	201,000	573	667
2	28,800	33.0	2.8	208,000	552	696

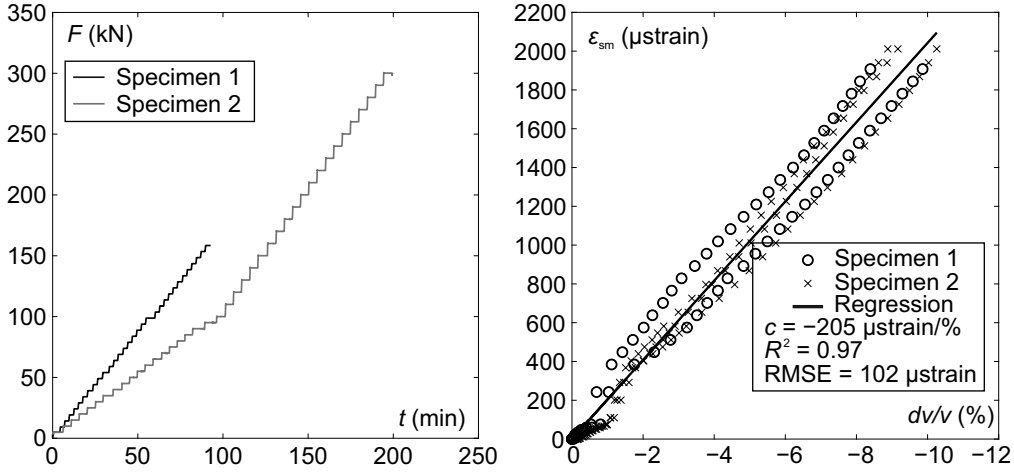

Figure 3. Left: Force vs. time diagram of test 1 and 2, Right: Average steel strain (analytical) vs. relative velocity change (experimental) to calibrate the model.

EXPERIMENTAL VALIDATION

Validation completes the proposed model for predicting reinforcement strains in cracked RC structures. Maximum steel strains in the crack predicted by the ε_s-dv/v model are compared with strains recorded with FOS at two load levels in figure 4. It should be noted that in test specimen 1, two US transducers failed during the test; their data are thus missing. At lower load levels (figure 4 top), the predictions slightly overestimate the actual maximum strain. At higher forces (figure 4 bottom), the model underestimates the actual strain.

For a comprehensive analysis of the model's accuracy, the measured maximum strain in the area of each US transducer is compared to the respective predicted strain. The comparison of all data yields a coefficient of determination of $R^2 = 0.85$ and an RMSE $=$ 303 μstrain. Consequently, the model provides accurate predictions of reinforcement strain.

CONCLUSIONS

A model capable of accurately predicting strains even in cracked RC structures using US coda waves is derived and proposed for practical application. It combines the well-established σ_s-ε_{sm} relationship with highly sensitive US coda waves and their changes to localize and quantify minute strains:

- It provides holistic monitoring of RC structures from the non-cracked, linear-elastic region through initial cracking to completed cracking. Its validity covers about 90% of the maximum load-bearing capacity.
- Through its derivation, it provides geometry-, material-, and reinforcement ratio–independent predictions of steel strains based on US measurements.
- Based on the average steel strain, it captures the maximum strain in cracks with convincing accuracy: $R^2 = 0.85$, RMSE $= 303$ μstrain. The maximum strain allows

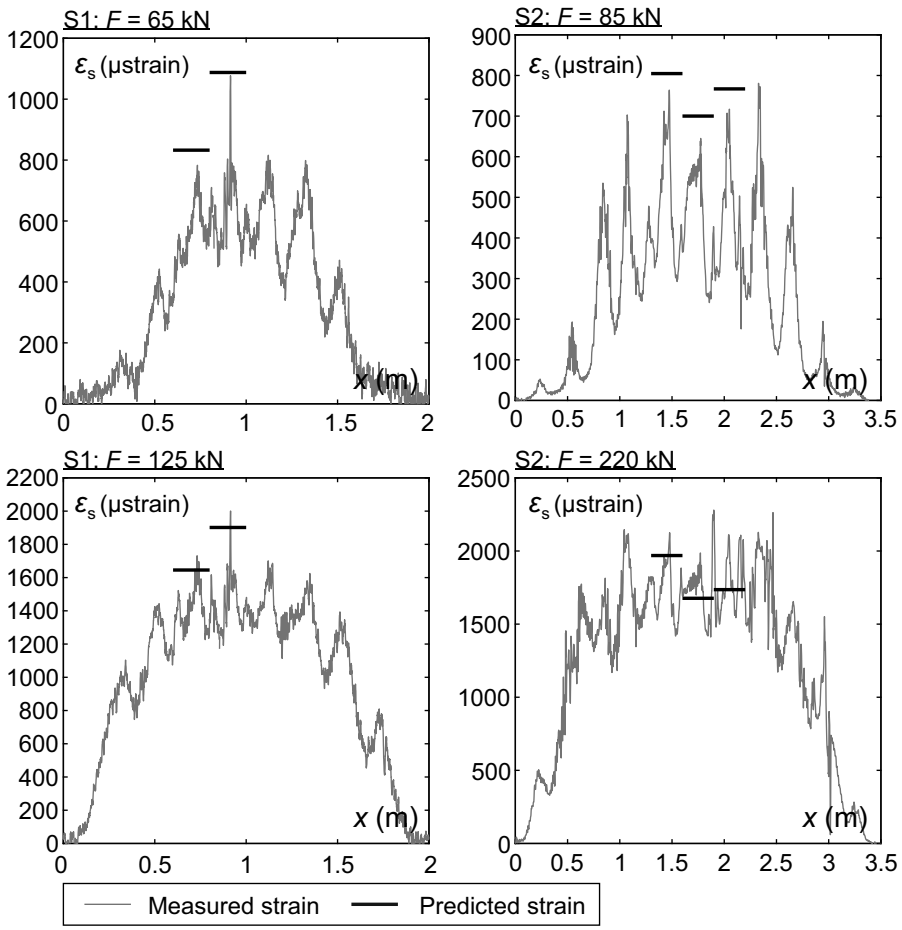

Figure 4. Comparison of model-predicted and fiber optical measured strains in the reinforcement.

direct inference on the utilization of the maximum load-bearing capacity and the steel stress in cracks.

ACKNOWLEDGMENT

Financial support provided by Deutsche Forschungsgemeinschaft (DFG, German Research Foundation [Project number 398216472]) is gratefully acknowledged.

REFERENCES

1. Poupinet, G., W. L. Ellsworth, and J. Frechet. 1984. "Monitoring velocity variations in the crust using earthquake doublets: An application to the Calaveras Fault, California," *Journal of Geophysical Research: Solid Earth*, 89(B7):5719–5731, doi:10.1029/JB089iB07p05719.
2. Diewald, F., N. Epple, T. Kraenkel, C. Gehlen, and E. Niederleithinger. 2022. "Impact of External Mechanical Loads on Coda Waves in Concrete," *Materials*, 15(16), doi:10.3390/ma15165482.
3. Clauß, F., N. Epple, M. A. Ahrens, E. Niederleithinger, and P. Mark. 2020. "Comparison of Experimentally Determined Two-Dimensional Strain Fields and Mapped Ultrasonic Data Processed by Coda Wave Interferometry," *Sensors (Basel, Switzerland)*, 20(14):1–16, doi:10.3390/s20144023.

4. Larose, E. and S. Hall. 2009. “Monitoring stress related velocity variation in concrete with a $2{\cdot}10^{-5}$ relative resolution using diffuse ultrasound,” *The Journal of the Acoustical Society of America*, 125(4):1853–1856, doi:10.1121/1.3079771.
5. Grabke, S., F. Clauß, K.-U. Bletzinger, M. A. Ahrens, P. Mark, and R. Wüchner. 2021. “Damage Detection at a Reinforced Concrete Specimen with Coda Wave Interferometry,” *Materials*, 14(17), doi:10.3390/ma14175013.
6. Grabke, S., K.-U. Bletzinger, and R. Wüchner. 2022. “Development of a finite element-based damage localization technique for concrete by applying coda wave interferometry,” *Engineering Structures*, 269:114585, doi:10.1016/j.engstruct.2022.114585.
7. Larose, E., A. Obermann, A. Digulescu, T. Planès, J.-F. Chaix, F. Mazerolle, and G. Moreau. 2015. “Locating and characterizing a crack in concrete with diffuse ultrasound A four-point bending test,” *The Journal of the Acoustical Society of America*, 138(1):232–241, doi:10.1121/1.4922330.
8. Niederleithinger, E. and C. Wunderlich. 2013. “Influence of small temperature variations on the ultrasonic velocity in concrete,” AIP, AIP Conference Proceedings, pp. 390–397.
9. Legland, J.-B., R. Théry, O. Abraham, G. Villain, O. Durnad, E. Larose, and V. Tournat. 2018. “Influence of moisture on the estimation of nonlinear parameters in concrete with Nonlinear ultrasonic Coda Wave Interferometry,” in *Proceedings of 12th European Conference on Non-Destructive Testing (ECNDT 2018)*, Gothenburg, Sweden.
10. Snieder, R. 2002. “Coda wave interferometry and the equilibration of energy in elastic media,” *Physical review E*, 66(4), doi:10.1103/PhysRevE.66.046615.
11. Clauß, F., N. Epple, M. A. Ahrens, E. Niederleithinger, and P. Mark. 2022. “Correlation of Load-Bearing Behavior of Reinforced Concrete Members and Velocity Changes of Coda Waves,” *Materials*, 15(3), doi:10.3390/ma15030738.
12. Niederleithinger, E., X. Wang, M. Herbrand, and M. Müller. 2018. “Processing Ultrasonic Data by Coda Wave Interferometry to Monitor Load Tests of Concrete Beams,” *Sensors (Basel, Switzerland)*, 18(6), doi:10.3390/s18061971.
13. Comité euro-international du béton. 1993. *CEB-FIP model code 1990: Design code*, vol. 213/214 of *Bulletin d’information / Comité Euro-International du Béton*, Telford, London, ISBN 978-0-7277-1696-5.
14. Zilch, K. and G. Zehetmaier. 2010. *Bemessung im konstruktiven Betonbau*, Springer Berlin Heidelberg, Berlin, Heidelberg, ISBN 978-3-540-70637-3, doi:10.1007/978-3-540-70638-0.
15. Konertz, D., J. Löschmann, F. Clauß, and P. Mark. 2019. “Fiber optic sensing of strain and temperature fields,” *Bauingenieur*, 94(7/8):292–300, doi:10.37544/0005-6650-2019-07-08-70.
16. Clauß, F., M. A. Ahrens, and P. Mark. 2021. “A Comparative Evaluation of Strain Measurement Techniques in Reinforced Concrete Structures – A Discussion of Assembly, Application, and Accuracy,” *Structural Concrete*, 22(5):2992–3007, doi:10.1002/suco.202000706.
17. Clauß, F., M. A. Ahrens, and P. Mark. “Thermo-mechanical experiments on reinforced concrete beams: Assessing thermal, mechanical, and mixed impacts on fiber optic measurements,” *Structural Concrete*, doi:10.1002/suco.202100890.